Performance Optimization of 2-PolSK in UV Scattering Communication Channels

Srishti Sharma and Swades De

Department of Electrical Engineering
Indian Institute of Technology Delhi, New Delhi, India

accepted in

IEEE Communication Letters

Outline

Introduction and Motivation

- Optical wireless communication has gained prominence due to the following:
  - abundant unregulated spectral resource
  - high data rates
  - immunity to electromagnetic interference
  - use of low power transceivers
- UV-C ($200 \sim 300$ nm) band is preferred over visible light (VL) and infrared (IR) at optical frequencies due to the following:
  - Solar blind feature at the ground level
  - Ability to communicate via non-line of sight (NLOS) paths
  - Scattering probability of UV light by the virtue of suspended particulate matter in the atmosphere is higher[1]
- UV NLOS propagation occurs due to strong molecular and aerosol scattering effects[2].
- The received power is higher in NLOS communication at UV frequency compared to other optical bands, thereby providing high SNR
- UV communication becomes an important military application when radio, wire or fiber communication links are unavailable or unreliable.

[1] C. Xu and H. Zhang, "Channel analyses over wide optical spectra for long-range scattering communication", *IEEE Commun. Lett.*, vol. 19, no. 2, pp. 187–190, 2015.

[2] D.M. Reilly, *et al.*, "Unique properties of solar blind ultraviolet communication systems for unattended ground sensor networks", in *Unmanned/Unattended Sensors and Sensor Networks*, SPIE, vol. 5611, 2004, pp. 244–254.

Related Works

- Various modulation techniques were proposed for UV NLOS communication: On-off keying (OOK), pulse position modulation (PPM)[3], and multi-PPM[4], digital and dual-head pulse interval[5], 4-frequency shift keying[6], orbital angular momentum[7], binary phase shift keying subcarrier intensity[8], and M-ary spectral amplitude code[9]
- Most of them have focused on amplitude and phase aspects of the electromagnetic (EM) wave

Limitation: Amplitude and angular-based modulation strategies are susceptible to path loss and phase noise, respectively

Polarization-aware UV NLOS communication is of interest because it is insensitive to path loss and phase noise; only sufficient power level is required for symbol detection.

[3] Z. Jiang, *et al.*, "Achievable rates and signal detection for photon-level photomultiplier receiver based on statistical non-linear model", *IEEE Trans. Wirel. Commun.*, vol. 18, no. 12, pp. 6015–6029, 2019. DOI: 10.1109/TWC.2019.2941477.

[4] T. Cao *et al.*, "Performance of multipulse pulse-position modulation in nlos ultraviolet communications", *IEEE Commun. Lett.*, vol. 27, no. 3, pp. 901–905, 2023.

[5] C. Xu and H. Zhang, "Packet error rate analysis of IM/DD systems for ultraviolet scattering communications", in *Proc. IEEE MILCOM*, 2015. DOI: 10.1109/MILCOM.2015.7357607.

[6] Y. Zhao, *et al.*, "Investigation of characteristics of ultraviolet light pulse weak signal communication system based on fourth-order frequency-shift keying modulation", in *Photonics*, vol. 11, 2024, p. 395.

[7] S. Arya and Y. H. Chung, "High-performance and high-capacity ultraviolet communication with orbital angular momentum", *IEEE Access*, vol. 7, pp. 116 734–116 740, 2019.

[8] L.Wang, *et al.*, "Non-line-of-sight ultraviolet link loss in noncoplanar geometry", *Optics letters*, vol. 35, no. 8, pp. 1263–1265, 2010.

[9] M. Noshad *et al.*, "NLOS UV communications using M-ary spectral-amplitude-coding", *IEEE Trans. Commun.*, vol. 61, no. 4, pp. 1544–1553, 2013.

Related Works (Contd.)

- The propagation of polarized light in scattering environments (turbid media, tissues) was studied using electric field Monte Carlo (EFMC)[10,11] simulations and MC-based Stokes-Muller transformations[12].
- They did not study the communication performance over the scattering channels.
- To address this lacuna, feasibility of NLOS polarized UV signal communication was studied[13].
- Dual modulated UV communication with intensity and polarization modulation was proposed[14].
- Polarization multiplexed communication was shown to increase data rate[15].
- Thus, combining the existing modulation schemes with 2-PolSK can double the achievable data rate.

Observation: Polarization-aware communication performance is affected by channel scattering, which has not been sufficiently studied in the literature.

Inference: Mitigating depolarization-induced degradation is crucial for communication performance enhancement in scattering channels.

---

[10] M. Xu, "Electric field monte carlo simulation of polarized light propagation in turbid media", *Opt. Express*, vol. 12, no. 26, pp. 6530–6539, 2004.

[11] A. Doronin *et al.*, "Two electric field monte carlo models of coherent backscattering of polarized light", *J. Opt. Soc. Am. A*, vol. 31, no. 11, pp. 2394–2400, 2014.

[12] L. Li , *et al.*, "Simulation of light scattering from a colloidal droplet using a polarized monte carlo method: Application to the time-shift technique", *Opt. Express*, vol. 27, no. 25, pp. 36 388–36 404, 2019.

[13] H. Yin, *et al.*, "Vectorized polarization-sensitive model of non-line-of-sight multiple-scatter propagation", *J. Opt. Soc. Am. A*, vol. 28, no. 10, pp. 2082–2085, 2011.

[14] H. Yin, *et al.*, "Extending the data rate of non-line-of-sight UV communication with polarization modulation", in *Unmanned/Unattended Sensors and Sensor Networks IX*, vol. 8540, SPIE, 2012, p. 85400I.

[15] Z. Hailiang *et al.*, "Characteristics of non-line-of-sight polarization ultraviolet communication channels", *Appl. Opt.*, vol. 51, no. 35, pp. 8366–8372, 2012.

Contributions and Significance

Contributions

1. XPD-based scattering channel characterization and XPD-dependent polarization orientation are mathematically captured.
2. Different scattering channel scenarios are defined in terms of polarization orientation variance, and conditions are obtained under which different-from-conventional symmetric thresholding is required for minimum error performance.
3. Optimal thresholding is decided by modeling the received polarization orientation as truncated Gaussian distributed. Expectation maximization (EM) algorithm is used to compute the modeled statistical parameters. Optimal thresholds are derived in terms of the statistical moments of the received signal polarization.
4. EFMC based polarized light propagation and condition for its reception are discussed, and the BER performance of the proposed optimal thresholding is compared with respect to the conventional symmetric thresholding.

Significance

This work is significant as it improves the communication performance of polarization modulation/ multiplexing in UV scattering channels.

System Model

- Modulation scheme: 2-PolSK
- Transmit electric field: $\mathbf{E}_t = [E_{th}, E_{tv}]^T$
- Source symbol vector: $\mathbf{s} = [s_h \;\; s_v]^T = \sqrt{P_t}\mathbf{E}_t s$
- Polarization sensitive scattering channel:
  $\mathbf{H} = [h_{hh} \;\; h_{hv}; h_{vh}, \;\; h_{vv}]$
- Received electric field: $\mathbf{E}_r = [E_{rh}, E_{rv}]^T = \sqrt{P_t l_p}\mathbf{H}\mathbf{s}$
- Received electrical signal: $\mathbf{x} = \sqrt{R}\mathbf{E}_r + \mathbf{n}$
  - Polarization orientation angle of the beam is $\psi_r = 0.5\tan^{-1}(I_{r2}/I_{r1})$, where $I_{r1} = x_h x_h^* - x_v x_v^*$ and $I_{r2} = x_h x_v^* + x_h^* x_v$ are the Stokes parameters.

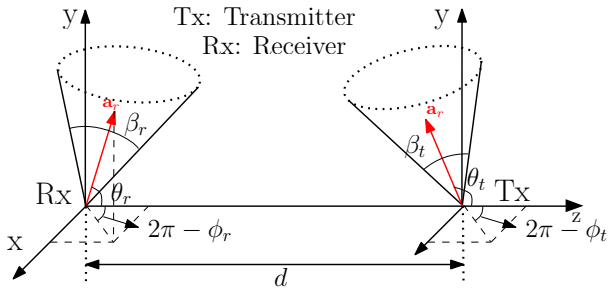

Figure 1: Geometrical setup for propagation of photon in scattering channel. TX: transmitter, Rx: receiver

Notations:
s: source symbol; l_p: path loss; P_t: transmit power; R: Optical to electrical conversion ratio
$\mathbf{n} = [n_h, n_v]^T$: AWGN vector with $n_h, n_v \sim \mathcal{CN}(0, \sigma_n^2)$

Remark

In this work, 2-PolSK is achieved by transmitting either horizontal (vector along x axis) or vertical (vector along y axis) polarization from the transmitter.

Scattering Channel Characterization

- Light propagation in scattering channel is described in terms of amplitude scattering matrix **S** which depends on the scatterer radius r_s, scatterer refractive index m, wavelength λ, scattering angle θ, and azimuth angle ϕ with respect to scattering plane[16,17].
- Polarization scattering channel matrix is written as

$$\mathbf{H} = \prod_{n=1}^{N} \mathbf{S}(\theta_n, \phi_n) \tag{1}$$

where N is the scattering order.

- $\mathbf{S}(\theta_i, \phi_i)$ denotes the scattered wave field propagating along the (θ_i, ϕ_i) direction given by[18].

$$\mathbf{S}(\theta_i, \phi_i) = \frac{1}{\sqrt{F(\theta_i, \phi_i)}} \begin{bmatrix} S_2(\theta_i)\cos\phi_i & S_2(\theta_i)\sin\phi_i \\ -S_1(\theta_i)\sin\phi_i & S_1(\theta_i)\cos\phi_i \end{bmatrix} \tag{2}$$

where the factor $F(\theta_i, \phi_i)$ is introduced to normalize the light intensity

[16] M. Xu, "Electric field monte carlo simulation of polarized light propagation in turbid media", *Opt. Express*, vol. 12, no. 26, pp. 6530–6539, 2004.

[17] W. J. Wiscombe, "Improved mie scattering algorithms", *Appl. Opt.*, vol. 19, no. 9, pp. 1505–1509, 1980.

[18] C. Xu and H. Zhang, "Channel analyses over wide optical spectra for long-range scattering communication", *IEEE Commun. Lett.*, vol. 19, no. 2, pp. 187–190, 2015.

Scattering Channel Characterization (Contd.)

- Statistical characterization of channel is done in terms of XPD which accounts for energy transfer between the orthogonal polarization states.
- Instantaneous horizontal and vertical XPD are defined as

$$\text{XPD}_h = \frac{|h_{hh}|^2}{|h_{vh}|^2} \quad \text{XPD}_v = \frac{|h_{vv}|^2}{|h_{hv}|^2}. \tag{3}$$

- Expressing channel matrix parameters in polar form as $h_{hh} = |h_{hh}|e^{j\phi_{hh}}$, $h_{hv} = |h_{hv}|e^{j\phi_{hv}}$, $h_{vh} = |h_{vh}|e^{j\phi_{vh}}$ and $h_{vv} = |h_{vv}|e^{j\phi_{vv}}$.
- Expressing the received Stokes parameters in terms of transmit field and channel parameters as

$$\begin{aligned}
I_{r1} &= \Big[\{|h_{hh}|^2 - |h_{vh}|^2\}\cos^2\psi_t + \{|h_{hv}|^2 - |h_{vv}|^2\}\sin^2\psi_t \\
&\quad + 2\cos\psi_t \sin\psi_t \{|h_{hh}||h_{hv}|\cos(\phi_{hh} - \phi_{hv}) - |h_{vh}||h_{vv}|\cos(\phi_{vh} - \phi_{vv})\}\Big]\cos^2\alpha_1, \\
I_{r2} &= 2\Big[|h_{hh}||h_{vh}|\cos^2\psi_t\cos(\phi_{hh} - \phi_{vh}) + |h_{hv}||h_{vv}|\sin^2\psi_t\cos(\phi_{hv} - \phi_{vv}) \\
&\quad + \cos\psi_t\sin\psi_t\left(|h_{hh}||h_{vv}|\cos(\phi_{hh} - \phi_{vv}) + |h_{12}||h_{21}|\cos(\phi_{hv} - \phi_{vh})\right)\cos^2\alpha_1.
\end{aligned} \tag{4}$$

- Received orientation for transmit horizontal and vertical polarization as

$$\psi_{rh} = \frac{1}{2}\tan^{-1}\left[\frac{2\sqrt{\text{XPD}_h}\cos(\phi_{hh} - \phi_{vh})}{\text{XPD}_h - 1}\right] \quad \psi_{rv} = \frac{1}{2}\tan^{-1}\left[\frac{2\sqrt{\text{XPD}_v}\cos(\phi_{hv} - \phi_{vv})}{1 - \text{XPD}_v}\right]. \tag{5}$$

Optimal 2-PolSK Decoding Thresholding

Different Scenarios in Scattering Communication

- Conventional 2-PolSK detection technique in optical wireless communication: *Symmetric thresholding*
- UV scattering channels are asymmetric: symmetric thresholding is not optimal
- We define the following cases:
  - **A** $\sigma_h^2 > \sigma_v^2$ or $\sigma_h^2 < \sigma_v^2$, $\sigma_h^2 \in [-\frac{\pi}{4}, \frac{\pi}{4}]$ and $\sigma_v^2 \in [\frac{\pi}{4}, \frac{3\pi}{4}]$; symmetric thresholds are sufficient
  - **B** $\sigma_h^2 > \sigma_v^2$, σ_h^2 crosses the region in range $[\frac{\pi}{4}, \frac{3\pi}{4}]$; optimal thresholds $\in [\frac{\pi}{4}, \frac{3\pi}{4}]$ through $\frac{\pi}{2}$
  - **C** $\sigma_h^2 < \sigma_v^2$, σ_h^2 crosses the region in range $[\frac{\pi}{4}, \frac{3\pi}{4}]$; optimal thresholds $\in [\frac{\pi}{4}, \frac{3\pi}{4}]$ through 0

Distribution Parameter Estimation

- Received polarization distributions are approximated as truncated Gaussian distributed
- ψ_r is defined on the circular scale; Gaussian distribution is suitably truncated in the range k_1 and k_2
- The corresponding probability density function (PDF) is

$$f_p(x|p, k_1, k_2) = \frac{\phi\left((x - \mu_p)/\sigma_p\right)}{\sigma_p Z_p} \tag{6}$$

- ϕ is the PDF of the standard normal distribution
  $p \in \{h, v\}$ indicates the transmitted signal polarization
  $Z_p = \Phi(\beta_p) - \Phi(\alpha_p)$ is the normalization constant
  $\alpha_p = \frac{k_1 - \mu_p}{\sigma_p}$ and $\beta_p = \frac{k_2 - \mu_p}{\sigma_p}$, μ_p and σ_p are the mean and variance of $\phi(\cdot)$
  $\Phi(x) = 0.5\left(1 + \text{erf}\left(x/\sqrt{2}\right)\right)$.

Optimal 2-PolSK Decoding Thresholding (Contd.)

- The log-likelihood function for the entire dataset $\{x_1, x_2, \cdots, x_N\}$ is:

$$\begin{aligned}\ln L(\{x_i\};\mu_p,\sigma_p) &= \sum_{i=1}^{N}\left[\ln\phi\left(\frac{x_i-\mu_p}{\sigma_p}\right)-\ln\sigma_p-\log Z_p\right] \\ &= -\frac{N}{2}\log(2\pi)-N\log\sigma_p-\sum_{i=1}^{N}\frac{(x_i-\mu_p)^2}{2\sigma_p^2}-N\log Z_p.\end{aligned} \tag{7}$$

- To estimate μ_p and σ_p, we maximize (7) and the corresponding optimization problem is formulated as

$$\begin{aligned}(\mathbf{P}1): \quad &\max_{\mu_p,\sigma_p} \ \ln L(\{x_i\};\mu_p,\sigma_p) \\ \mathbf{C}1: \quad &\sigma_p > 0.\end{aligned} \tag{8}$$

  ($\mathbf{P}1$) is nonlinear.
- The solution employs the EM algorithm to obtain the optimal model parameters: μ_h, σ_h, μ_v, σ_v.

Optimal 2-PolSK Decoding Thresholding (Contd.)

The EM algorithm steps are as follows:

1. **E**-step: Given current estimates $\mu_p^{(t)}$ and $\sigma_p^{(t)}$, the expected values (adjustments) for mean and variance that account for the missing tails are:
   - Mean adjustment: $\Delta\mu_p = (\phi(\alpha_p^{(t)}) - \phi(\beta_p^{(t)}))/Z_p^{(t)}$
   - Variance adjustment: $\Delta\sigma_p = \frac{\alpha_p^{(t)}\phi(\alpha_p^{(t)}) - \beta_p^{(t)}\phi(\beta_p^{(t)})}{Z_p^{(t)}} + 1 - \Delta\mu_p^2$ where $\alpha_p^{(t)} = (k_1 - \mu_p^{(t)})/\sigma_p^{(t)}$, $\beta_p^{(t)} = (k_2 - \mu_p^{(t)})/\sigma_p^{(t)}$, and $Z_p^{(t)} = \Phi(\beta_p^{(t)}) - \Phi(\alpha_p^{(t)})$.
2. **M**-step: Using the adjustments from the E-step we update μ_p and σ_p to increase the likelihood.
   - Update μ_p: $\mu_p^{(t+1)} = \mu_p^{(t)} - \sigma_p^{(t)} \cdot \Delta\mu_p$
   - Update σ_p: $\sigma_p^{(t+1)} = \{\sum_{i=1}^{N}(x_i - \mu_p^{(t+1)})^2/N\Delta\sigma_p\}^{\frac{1}{2}}$
3. Convergence: The algorithm iterates between the E and M steps until the changes in μ_p and σ_p are less than a tolerance level, or a maximum iteration count is reached.

Remark

Probabilistic modeling of the received polarization orientation distribution can be done using the truncated Gaussian mixture model (TGMM) as well. The choice between TGMM and TGM is purely based on the trade-off between modeling accuracy and computational complexity. We observed that TGM achieves modeling accuracy close to that of the TGMM with significantly lower computational complexity.

Optimal 2-PolSK Decoding Thresholding (Contd.)

Estimation of Optimal 2-PolSK Decoding Thresholding

- All angles are computed in range $[0, \pi]$; optimal thresholds are defined within this range (Fig. 2 (a)).
- Domain set of the decision boundary is divided in two subsets of range $[0, \frac{\pi}{2}]$ and $[\frac{\pi}{2}, \pi]$ (Fig. 2(b)) and the cutoffs are calculated individually.

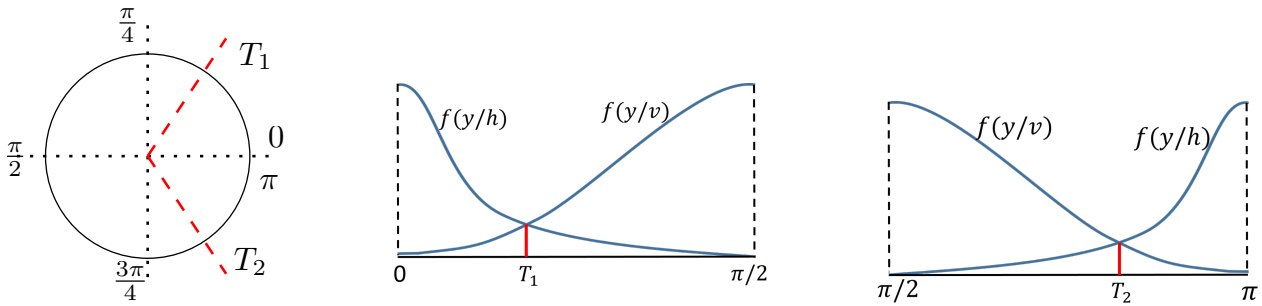

(a) (b) (c)

Figure 2: (a) A plane of Poincare sphere where polarization orientation varies from 0 to π. Decision boundary divided in subsets: (b) $[0, \pi/2]$, (c) $[\pi/2, \pi]$.

- The probability of error for the subset in the range $[0, \frac{\pi}{2}]$ is given by

$$P_{e1} = p(v) \int_0^{T_1} f_v(y|v)dy + p(h) \int_{T_1}^{\pi/2} f_h(y|h)dy \tag{9}$$

where $p(v)$ and $p(h)$ are the steady-state probabilities of vertical and horizontal polarization, respectively.

Optimal 2-PolSK Decoding Thresholding (Contd.)

- Probability of error for the subset in the range $[\pi/2, \pi]$ is obtained similarly by minimizing

$$P_{e2} = p(v)\int_{\pi/2}^{T_2} f_v(y|v)dy + p(h)\int_{T_2}^{\pi} f_h(y|h)dy. \tag{10}$$

- Optimal Thresholds are given by

$$T_j^{opt} = \frac{\pm 2\left[(\mu_h\sigma_v^2 - \mu_v\sigma_h^2)^2 - (\mu_v^2\sigma_h^2 - \mu_h^2\sigma_v^2 - M_j)(\sigma_h^2 - \sigma_v^2)\right]^{1/2} - 2(\mu_h\sigma_v^2 - \mu_v\sigma_h^2)}{(2(\sigma_h^2 - \sigma_v^2))}, j \in \{1, 2\} \tag{11}$$

- where M_1 and M_2 are given by

$$M_1 = 2\ln\left[\frac{\sigma_v p(v)\left[\text{erf}\left(\frac{\pi/2-\mu_v}{\sqrt{2}\sigma_v}\right) - \text{erf}\left(\frac{-\mu_v}{\sqrt{2}\sigma_v}\right)\right]}{\sigma_h p(h)\left[\text{erf}\left(\frac{\pi/2-\mu_h}{\sqrt{2}\sigma_h}\right) - \text{erf}\left(\frac{-\mu_h}{\sqrt{2}\sigma_h}\right)\right]}\right]$$
$$M_2 = 2\ln\left[\frac{\sigma_v p(v)\left[\text{erf}\left(\frac{\pi-\mu_v}{\sqrt{2}\sigma_v}\right) - \text{erf}\left(\frac{\pi/2-\mu_v}{\sqrt{2}\sigma_v}\right)\right]}{\sigma_h p(h)\left[\text{erf}\left(\frac{\pi-\mu_h}{\sqrt{2}\sigma_h}\right) - \text{erf}\left(\frac{\pi/2-\mu_h}{\sqrt{2}\sigma_h}\right)\right]}\right] \tag{12}$$

Electric Field Monte-Carlo Simulation

Photon Propagation and Field Updation

- In EFMC, scattering takes place in local coordinate system (**p**, **q**, **r**) at each iteration step.
- The scattering (elevation) angle θ and azimuth angle ϕ are measured with respect to the direction of incidence of photon on the scatterer.
- Position update of the i-th scatterer: $\mathbf{s}_i = \mathbf{s}_{i-1} + d_{i-1}\mathbf{r}_{i-1}$
- The update rule for the bases of the local coordinates system at each scattering is governed by $[\mathbf{p}' \quad \mathbf{q}' \quad \mathbf{r}'] = A(\theta, \phi)[\mathbf{p} \quad \mathbf{q} \quad \mathbf{r}]$ where

$$A(\theta, \phi) = \begin{bmatrix} \cos\phi & \sin\phi\sin\theta & \sin\phi\cos\theta \\ 0 & \cos\theta & -\sin\theta \\ -\sin\phi & \sin\theta\cos\phi & \cos\theta\cos\phi \end{bmatrix}. \tag{13}$$

- Scattering angle distribution in free space UV communication is

$$f_\Theta(\theta_i) = \frac{{k_s}^R}{k_s} {f_\Theta}^R(\theta_i) + \frac{{k_s}^M}{k_s} {f_\Theta}^M(\theta_i), \quad 0 \le \theta_i \le \pi. \tag{14}$$

- Scattering coefficient under Rayleigh and Mie scattering is defined as

$$k_s = {k_s}^R + {k_s}^M, \tag{15}$$

${k_s}^R$ and ${k_s}^M = N_d Q_s \pi r_s^2$ are the molecule (Rayleigh) and aerosol (Mie) scattering coefficient, respectively. Q_s is the scattering cross-section given in[19].

[19] C. Xu *et al.*, "Effects of haze particles and fog droplets on NLOS ultraviolet communication channels", *Opt. Express*, vol. 23, no. 18, pp. 23 259–23 269, 2015.

Electric Field Monte-Carlo Simulation (Contd.)

- The phase function for Rayleigh and Mie scattering are

$$f_{\Theta}^{R}(\theta_i) = \frac{3[1+3\gamma+(1-\gamma)\cos^2\theta_i]}{8(1+2\gamma)}\sin\theta_i, \tag{16}$$

$$f_{\theta}^{M}(\theta_i) = \frac{1-g^2}{2}\left[\frac{1}{(1+g^2-2g\cos\theta_i)^{\frac{3}{2}}} + f\frac{0.5(3\cos^2\theta_i-1)}{(1+g^2)^{\frac{3}{2}}}\right]\sin\theta_i \tag{17}$$

- As the value of g increases, forward scattering becomes stronger[20].
- Propagation distance d_i for i^{th} scattering is distributed as

$$f_D(d_i) = k_e e^{-k_e d_i}, \qquad 0 \le d_i \le \infty \tag{18}$$

- The scattered field propagating along (θ_i, ϕ_i) direction is given by

$$\begin{bmatrix} E_{h,i+1} \\ E_{v,i+1} \end{bmatrix} = \mathbf{S}(\theta_i, \phi_i) \begin{bmatrix} E_{h,i} \\ E_{v,i} \end{bmatrix} \tag{19}$$

[20] H. Ding *et al.*, "Modeling of non-line-of-sight ultraviolet scattering channels for communication", *IEEE J. Sel. Areas Commun.*, vol. 27, no. 9, pp. 1535–1544, 2009.

Electric Field Monte-Carlo Simulation (Contd.)

Conditions for Photon Reception

$$
\begin{aligned}
C1: &\quad \cos^{-1}(\mathbf{a}_R.(-\mathbf{r}_i)) \leq \beta_R/2 && \textit{related to the receiver material property}\\
C2: &\quad d_i < l_m && \textit{ensures that photon doesn't meet any scatterer in the FOV}\\
C3: &\quad ||\mathbf{s}_i + d_i\mathbf{r}_i||_2 \leq A_r && \textit{ensures that the photon falls within the receiver area.}
\end{aligned}
$$

Polarization of Received Photon

- Projection of the polarization plane of the i-th received photon on the receiver plane is

$$\mathbf{E}_r = \begin{bmatrix} E_{hi} & E_{vi} \end{bmatrix}^T \cos\alpha_1 \tag{20}$$

  where α_1 is the angle between the polarization plane of the received photon and the receiver plane.
- From $\mathbf{E}_r$, we compute the Stokes parameters which in turn gives the polarization of detected photon.

Considering the short-range polarization assisted communication, we neglect the turbulence effects of the channel as polarization is negligibly impacted by turbulence in optical channel [6,7].

[21] D. H. Höhn, "Depolarization of a laser beam at 6328 å due to atmospheric transmission", *Appl. Opt.*, vol. 8, no. 2, pp. 367–369, 1969.

[22] J. Zhang, *et al.*, "Theoretical and experimental studies of polarization fluctuations over atmospheric turbulent channels for wireless optical communication systems", *Opt. Express*, vol. 22, no. 26, pp. 32 482–32 488, 2014.

Result: Performance in Two Different Channel Scenarios

- Two cases are observed for the simulation parameters in Table I
- In Fig. 3(a) corresponds to Case A as two distributions are far apart and symmetric thresholds are sufficient for signal detection.
- Fig. 3(b) corresponds to case C as the two distributions have unequal variance and optimum thresholding is required.
- Henceforth we consider the case C for performance optimization via optimal thresholding scheme

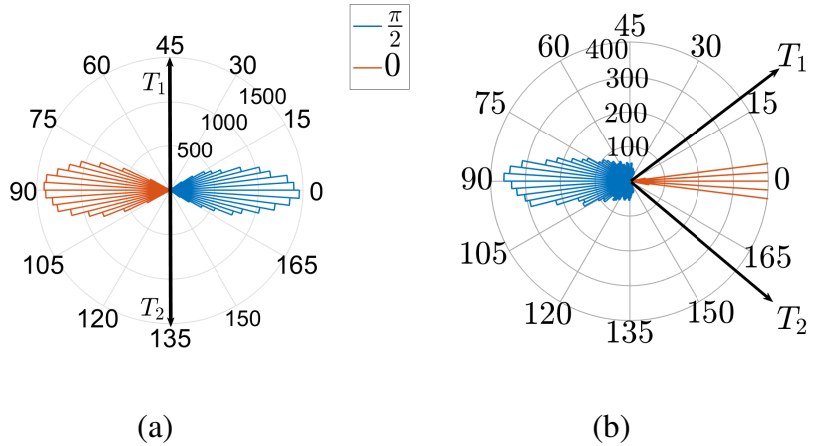

(a) (b)

Figure 3: Two different scattering channel scenarios observed for the simulation parameters in Table I: (a) case A ($\theta_t = 40^\circ$, $\theta_r = 140^\circ$), (b) case C ($\theta_t = 45^\circ$, $\theta_r = 135^\circ$). HP: horizontal polarization, VP: vertical polarization

Table 1: SIMULATION PARAMETERS

Variable	Value	Variable	Value	Variable	Value
β_t	10^o	A_r	$1.77\ \text{cm}^2$	P_t	20 mW
m	1.5	λ	250 nm	N	1
r_s	280 nm	N_d	$10^9\ \text{m}^{-3}$	f[23]	0.72
ϕ_t, ϕ_r	0°	k_s^R	$0.328\ \text{km}^{-1}$	γ[24]	0.0172
d	800 m				

[23] R. Yuan *et al.*, "Monte-carlo integration models for multiple scattering based optical wireless communication", *IEEE Trans. Commun.*, vol. 68, no. 1, pp. 334–348, 2020. DOI: 10.1109/TCOMM.2019.2952135.

[24] R. Yuan *et al.*, "Monte-carlo integration models for multiple scattering based optical wireless communication", *IEEE Trans. Commun.*, vol. 68, no. 1, pp. 334–348, 2020. DOI: 10.1109/TCOMM.2019.2952135.

Result: Comparison of Original and Modeled Distribution

- $\psi_r \in [0, \pi]$ and do not extend till infinity.
- The received polarization orientation angles are considered to be truncated Gaussian distributed.
- Gaussian modeling is still done as the distribution in (6) takes the mean and variance of the Gaussian distribution which is truncated.
- Distributions are generated for FOV $= 30^o$ and SNR $= 36$ dB.
- Gaussian modeling is done with the objective to cover the extreme points in the main lobe.
- The values in the Poincare sphere which lie in the other half must be truncated.

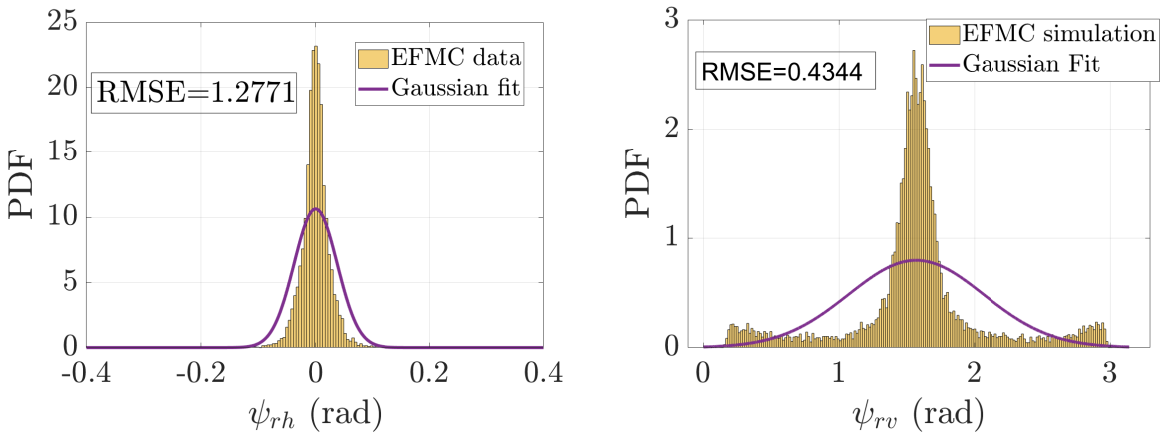

(a) (b)

Figure 4: Gaussian fit to the received polarization distribution with transmit polarization as (a) horizontal and (b) vertical.

Remark

To keep the distribution of ψ_r symmetric about 0 and $\frac{\pi}{2}$ radians, we plot distribution for ψ_{rh} and ψ_{rv} in the range $[\frac{-\pi}{2}, \frac{\pi}{2}]$ and $[0, \pi]$ respectively, as shown in Fig. 4.

Result: Variation of Polarization Orientation with XPD

- Curves are drawn for different values of $\Delta\phi_h = \phi_{hh} - \phi_{vh}$ and $\Delta\phi_v = \phi_{hv} - \phi_{vv}$.
- When horizontal polarization is transmitted, XPD_h is defined.
- When vertical polarization is transmitted, XPD_v is defined.
- For $XPD_h = 0$ dB, equal power is divided between the orthogonal components, i.e., $\psi_{rh} = \frac{\pi}{4}$.
- As XPD improves received ψ_{rh} decreases, reduces to zero at large XPD values.
- Similar trend is observed for vertical polarization orientation

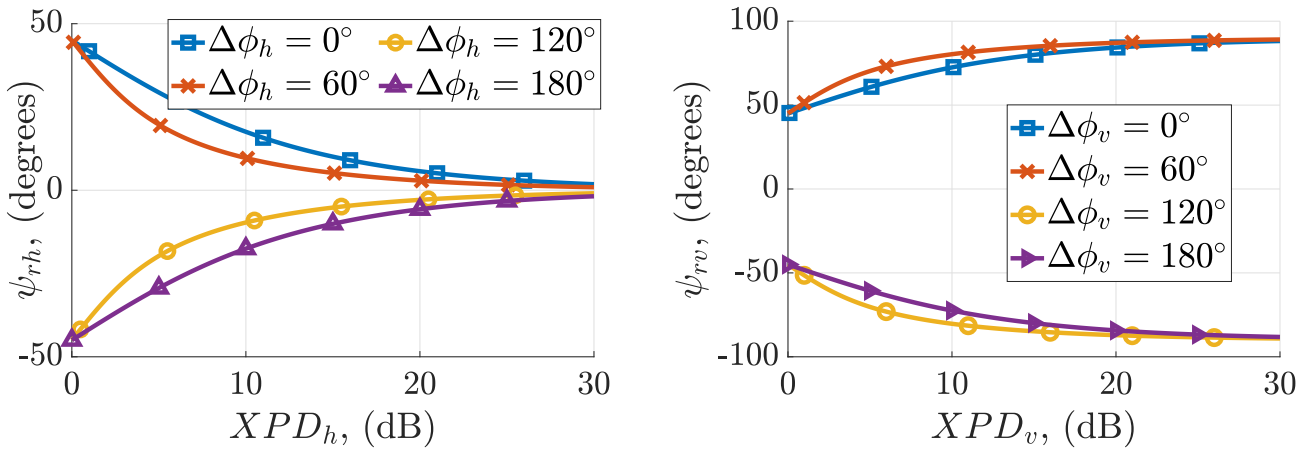

Figure 5: Variation of ψ_r with XPD with transmit polarization as (a) horizontal and (b) vertical.

Result: Impact of Change in Elevation Angle

- As polarization is direction-sensitive, the impact of elevation angle on channel XPD and variance of ψ_r are also observed
- The elevation angle of the transmitter and receiver are altered simultaneously.
- As the elevation angle increases, average XPD_h and XPD_v decreases for two different FOV
- $\text{XPD}_v < \text{XPD}_h$ is observed; dependent on the channel parameters considered
- As XPD increases, the polarization orientation variance decreases indicating an improvement in the scattering channel from polarization aspect

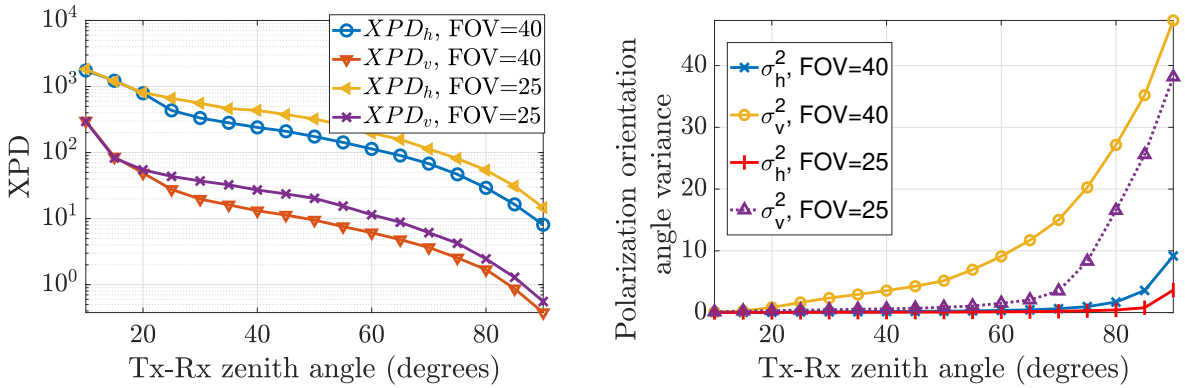

(a) (b)

Figure 6: Impact of change in elevation angle on (a) channel XPD, (b) polarization orientation angle variance.

Results: BER Performance

- Performance comparison of optimum and symmetric thresholds with $\theta_t = \pi - \theta_r = 45^\circ$
- BER curves show different trends when optimal thresholding method is employed for detection.
- For low FOV, BER approaches zero with an increase in SNR; BER is completely dependent on the receiver noise.
- For large FOV, it saturates at a high SNR level; BER is dependent on both receiver noise and channel.
- With the increase of FOV, achievable BER decreases.

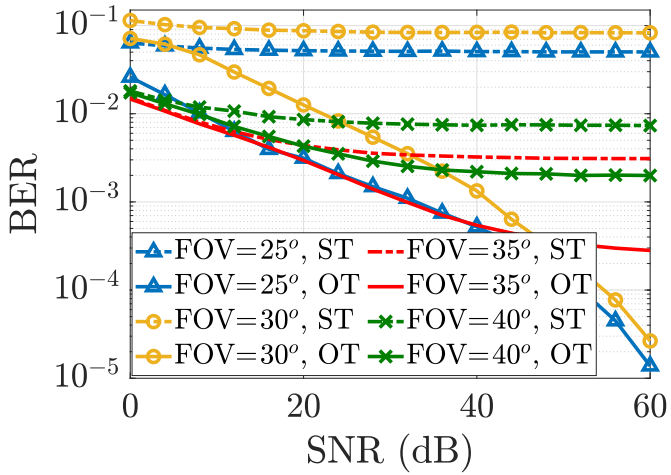

Figure 7: BER versus SNR performance for different receiver FOV. ST: Symmetric thresholding, OT: Optimal thresholding.

Conclusion

- Performance improvement of 2-PolSK scheme is proposed in NLOS UV scattering channel.
- Signal polarization-dependent channel XPD plays a crucial role in optimum thresholding for efficient polarization multiplexed signal communication
- Optimum thresholding scheme is proposed by approximating the received polarization orientation as truncated Gaussian distributed.
- EFMC simulation is used in NLOS UV scattering communication channel to realize the scattering scenario.
- The performance of optimal thresholding scheme is also compared with the conventional symmetric thresholding scheme in optical wireless communication
- The findings of this study will be useful in increasing the capacity of the UV scattering channels for polarization multiplexed transmissions.

Thank You